ADVANCES IN ATMOSPHERIC SCIENCES, VOL. 29, NO. 3, 2012, 635–645

Impact of Precursor Levels and Global Warming on Peak Ozone Concentration in the Pearl River Delta Region of China

WEI Xiaolin[1,2] (魏晓琳), LIU Qian[2] (刘 倩), Ka Se LAM*[2] (林嘉仕), and WANG Tijian[3] (王体健)

[1]*Meteorological Bureau of Shenzhen Municipality, Shenzhen* 518040

[2]*Department of Civil and Structural Engineering, The Hong Kong Polytechnic University, Hong Kong*

[3]*School of Atmospheric Science, Nanjing University, Nanjing* 210093

(Received 8 September 2011; revised 11 November 2011)

ABSTRACT

The relationship between the emission of ozone precursors and the chemical production of tropospheric ozone (O_3) in the Pearl River Delta Region (PRD) was studied using numerical simulation. The aim of this study was to examine the volatile organic compound (VOC)- or nitrogen oxide (NO_x =NO+NO_2)-limited conditions at present and when surface temperature is increasing due to global warming, thus to make recommendations for future ozone abatement policies for the PRD region. The model used for this application is the U.S. Environmental Protection Agency's (EPA's) third-generation air-quality modeling system; it consists of the mesoscale meteorological model MM5 and the chemical transport model named Community Multi-scale Air Quality (CMAQ). A series of sensitivity tests were conducted to assess the influence of VOC and NO_x variations on ozone production. Tropical cyclone was shown to be one of the important synoptic weather patterns leading to ozone pollution. The simulations were based on a tropical-cyclone-related episode that occurred during 14–16 September 2004. The results show that, in the future, the control strategy for emissions should be tightened. To reduce the current level of ozone to meet the Hong Kong Environmental Protection Department (EPD) air-quality objective (hourly average of 120 ppb), emphasis should be put on restricting the increase of NO_x emissions. Furthermore, for a wide range of possible changes in precursor emissions, temperature increase will increase the ozone peak in the PRD region; the areas affected by photochemical smog are growing wider, but the locations of the ozone plume are rather invariant.

Key words: chemical transport models, NO_x/VOC-limited conditions, photochemical reactivity, global warming

Citation: Wei, X. L., Q. Liu, K. S. Lam, and T. J. Wang, 2012: Impact of precursor levels and global warming on peak ozone concentration in the Pearl River Delta region of China. *Adv. Atmos. Sci.*, **29**(3), 635–645, doi: 10.1007/s00376-011-1167-4.

1. Introduction

Air pollution has become one of the most important and challenging issues for megacities worldwide. The air quality in the Pearl River Delta (PRD) region of China has been characterized by episodes of high surface ozone (O_3) levels which have often exceeded the health standard (Wang, 2003, 2006; Jiang, 2008, 2010). The high O_3 concentration originated from photochemical reactions of volatile organic compounds (VOCs) and nitrogen oxides (NO_x=NO+NO_2) under sunlight. Other processes, such as horizontal and vertical advection, transport, and deposition, also have significant roles in O_3 formation and depletion in the planetary boundary layer. At present, the critical issue in the control of ground-level O_3 pollution is to identify the relationship of O_3 production with its variations in precursor emissions, that is, whether this relationship is VOC limited or NO_x limited (NRC, 1991).

*Corresponding author: Ka Se LAM, cekslam@polyu.edu.hk

The application of various emissions reduction policies is a long-term endeavor. Previous works (Johnson et al., 1999; Hogrefe et al., 2004; Mickley et al., 2004; Leung and Gustafson, 2005) have indicated that using current meteorological conditions to determine future air quality is no longer sufficient. Significant changes in global and regional climate could affect meteorological conditions in the future; thus, the emission reduction policies aimed at reducing the negative impacts of ozone should account for this potential change. The average global air temperature has increased by 0.76°C over the past century, and it is predicted to increase further by 1.8°C–4.0°C in the coming century (IPCC, 2007). Climate change has significant impact on air pollution on global and/or regional scales (Jacob et al., 2009). So far, there have been few peer-reviewed studies reporting the impact of temperature increase on the ozone production efficiency (OPE) in the PRD region of China. The aim of this study was to examine the VOC- or NO_x-limited conditions at present and in the future when surface temperatures increase and to make recommendations for future ozone abatement policies for the PRD region. We studied O_3 concentrations under different VOC and NO_x emission scenarios and under different surface temperatures.

In this study, we evaluated the effects of changes in O_3 precursor emissions and air temperature on the gas-phase chemistry in the PRD region. Input data and the methodology of the simulation study are described in section 2. Subsequently, computed results of this study and data analyses are discussed in section 3. Conclusions are summarized in the last section.

2. Methodology

We used a chemical transport model to study the chemical production of O_3 in the troposphere under different VOC and NO_x emission scenarios. We then repeated the analysis with increased ground and air temperatures. The simulation was based on a tropical-cyclone-related regional ozone episode that occurred between 14 and 16 September 2004.

2.1 *Model configuration*

The chemical transport model named Community Multi-scale Air Quality (CMAQ) was used in this study. It is a three-dimensional air-quality model developed by the U.S. Environmental Protection Agency (EPA; Byun and Ching, 1999). In this study, we focused on gas-phase chemistry, which is represented by the carbon bond CB-4 chemical mechanism (Gery et al., 1989).

The MM5 meteorological model provided the meteorological input to the CMAQ. The domain configuration is the same as domain 1 of our previous study (Wei et al., 2007), which covered the whole of China and East Asia. The simulation started at 1200 LST 13 September 2004, and the duration was 85 h in total. With 12 h of model spin-up, simulation results from 0000 LST 14 September 2004 to 0000 LST 17 September 2004 were analyzed. During this summertime ozone episode, a tropical low-pressure system persisted in the South China Sea for 3 days. The relatively high temperature, weak wind, and stagnation conditions favored the accumulation of precursors and the generation of high O_3 levels. Because of the large computational domain and a long computation time, the horizontal resolution of the grid in this study was 81 km.

2.2 *Emission inventory*

In this study, we basically used the regional inventory for anthropogenic and biomass burning emissions compiled by Streets et al. (2003). However, there is compelling evidence that the carbon monoxide (CO) and NO_x were underestimated in this inventory, particularly for central and south China (Carmichael et al., 2003; Palmer et al., 2003). In this study, the emission inventory was adjusted according to Wang et al. (2004), who used an inversion model analysis. CO and NO_x in North China (35°–41.3°N, 190°–124°E) were increased by 24% and 47%, respectively. In central China (28.1°–35°N, 109°–123°E) the increase was 75% for CO and 189% for NO_x. For South China (17°–28.1°N, 109°–116°E), the increases were 88% for CO and 47% for NO_x. Apart from these adjustments, no other modifications on emissions were made.

The biogenic emissions were estimated using the Biogenic Emissions Inventory System version 3.09 (BEIS 3.09) algorithms in Sparse Matrix Operator Kernel Emissions (SMOKE) model system (Houyoux et al., 2000). Leaf temperature, pressure, and cloud-cover fraction as a function of both time and location required by the derivation of the BVOCs were output from the meteorology–chemistry interface processor (MCIP), which links meteorological models MM5 with the chemical transport model of the CMAQ modeling system. All vegetation types and density data required to predict biogenic emissions in SMOKE were generated using 30-s USGS data (ftp://ftp.ucar.edu/mesouser/MM5V3/TERRAIN_DATA/). In total, seven biogenic species were estimated using the SMOKE model system, namely isoprene (ISOP), terpene (TERPB), paraffin carbon bond (PAR), high molecular weight aldehydes (ALD2), and olefinic carbon bond (OLE), non-reactive carbon (NR), and NO.

Table 1. Maximum concentration of O_3 obtained in the CMAQ at 15 h (HK local time) and throughout the day. FVOC and FNO_x denote the factors applied to augment or reduce VOC and NO_x emissions for each simulation.

			Without temperature increase			With temperature increase		
Run no.	FVOC	FNO_x	Max. O_3 at 15 LST	Daily max. O_3	Max. hour	Max. O_3 at 15 LST	Daily max. O_3	Max. hour
R1	0.1	0.1	87	98	16	114	128	16
R2	0.1	1	143	185	17	184	266	17
R3	0.1	10	55	57	16	57	58	16
R4	10	0.1	65	67	16	82	82	15
R5	10	2	264	301	16	335	381	16
R6	1	0.1	78	82	16	97	100	16
R7 (base case)	1	1	270	270	14	301	301	14
R8	1	10	310	499	16	584	629	16
R9	1	2	414	415	15	490	490	14
R10	1	4	595	606	15	741	741	14
R11	2	10	860	860	14	996	996	14
R12	2	20	475	756	16	855	875	16
R13	30	10	416	428	15	499	499	14
R14	3	10	799	799	14	868	873	13
R15	3	30	612	910	16	1042	1042	14

2.3 *Sensitivity analysis and global warming scenario setup*

In total, a series of 15 simulation runs were performed. Whereas the meteorological conditions remained constant, the VOC and NO_x emissions were varied in each run. The factors applied in each run are shown in Table 1. The simulations were designed to study the change in peak O_3 due to different VOC and NO_x emission scenarios. The explored range of VOC and NO_x emissions was large enough to facilitate the construction of ozone isopleths that distinguish the VOC- and NO_x-limited regions (Toro et al., 2006).

The global mean temperature at the Earth's surface is expected to rise. To study the implication of future temperature increase on O_3 production, we re-ran all 15 cases with 10% increases in both air and ground temperatures, while the spatial temperature distribution pattern was unchanged. The 10% increase was, strictly speaking, arbitrary. It was chosen based on the existing air temperature range of 22°C–34°C in the PRD region. The 10% increase resulted in a temperature increase of 2.2°C–3.4°C, which is consistent with the predicted 1.8°C–4°C increase in global average air temperature by the end of the current century (IPCC, 2007). It should be noted that this temperature adjustment was the only change applied to the MM5 meteorological output, which was subsequently utilized in the CMAQ model. Therefore, the temperature change was applied in an uncoupled manner and did not affect other physical parameters, such as wind speed, wind direction, or the boundary-layer height. The only impact of temperature in these simulations occurred via the chemical kinetic reaction rates. Other temperature interactions, such as those that could alter emissions or other physical atmospheric properties, were not considered in this study. This methodology of accounting for global temperature increase is similar to that used by Steiner et al. (2006).

3. Results and discussion

3.1 *Model performance*

The map of PRD region and Hong Kong and the air-quality observation stations are shown in Fig. 1. Figure 2 shows the O_3 feature of the studied episode and the corresponding modeled result (Run7 in Table 1). First, although the resolution is relatively coarse

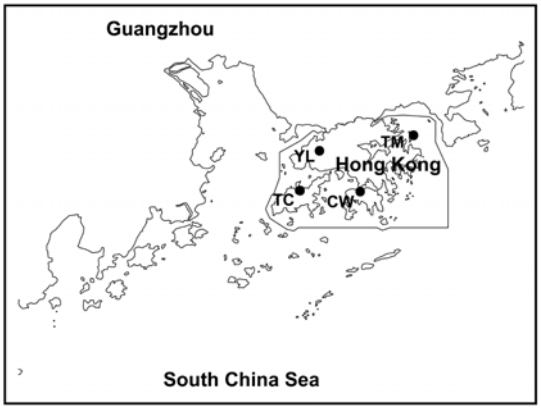

Fig. 1. Map of PRD region and Hong Kong, the air-quality observation stations as shown in black points.

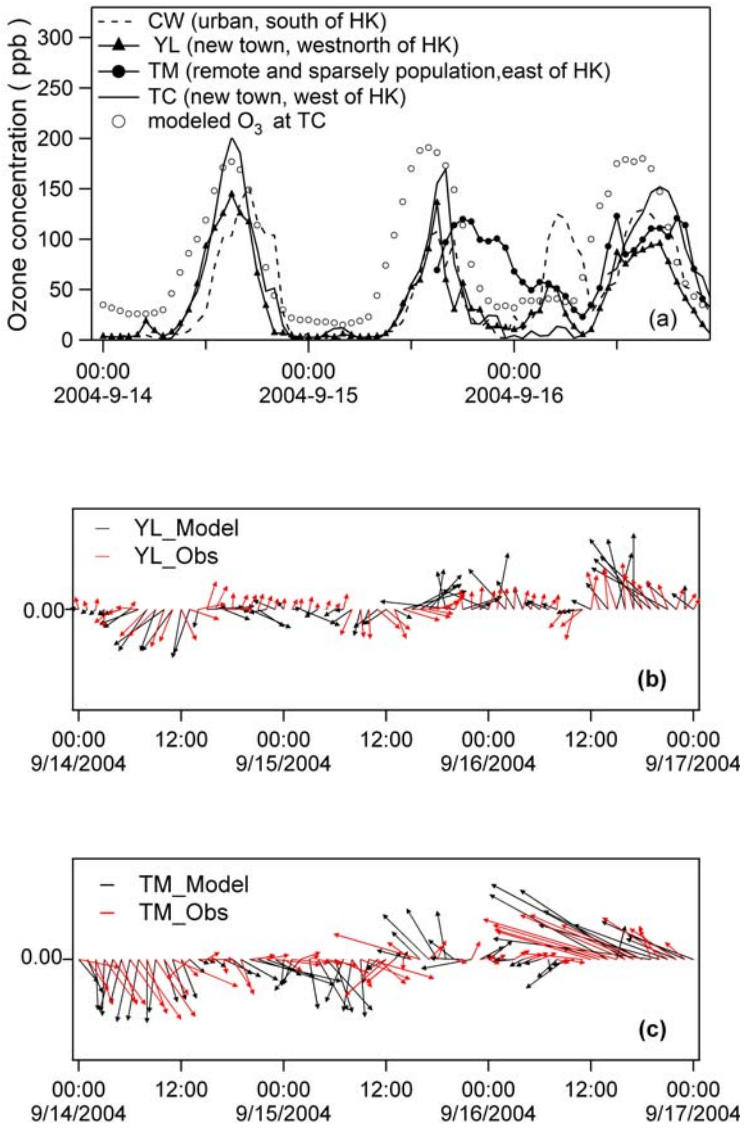

Fig. 2. Observed and corresponding simulated surface for (a) ozone concentration and (b, c) wind vector.

at 81 km, it shows that the simulation basically reproduced the O_3 peak that matches the O_3 peak observed in Tung Chung (a new town located in the western part of Hong Kong), except for the timing of ozone peaks on 15 and 16 September in the simulation. Second, this O_3 episode was regional; high O_3 levels were detected in almost the entire territory of Hong Kong. All the air-quality monitoring stations located at different areas, urban and suburban, recorded O_3 concentrations exceeding 100 ppb (see Fig. 2) in daytime during this event. The peak concentrations of O_3 were recorded at other monitoring stations: Central Western (CW), Yuen Long (YL), Tap Mun (TM) (Fig. 2). On both 14 and 16 September, the O_3 concentration reached nearly 150 ppb at the urban station CW. Even at the rural station TM, which is sparsely populated with very few anthropogenic emissions, the O_3 concentration exceeded 100 ppb on both 15 and 16 September.

Another distinctive feature of this episode was the wind field. Two features were observed: the diurnal change in wind direction and the slow rotation of wind before and after the episode. The local wind at YL was typically dominated by a northerly vector in the morning that switched to southerly direction in the afternoon on all 3 days, 14, 15, and 16 September 2004 (Fig. 2b). Both the local wind at the rural station TM (Fig. 2c) and the simulated regional wind (Figs. 3a and c) show the wind change from northerly to southeasterly during these 3 days.

Our hypothesis was that the O_3 was formed in the

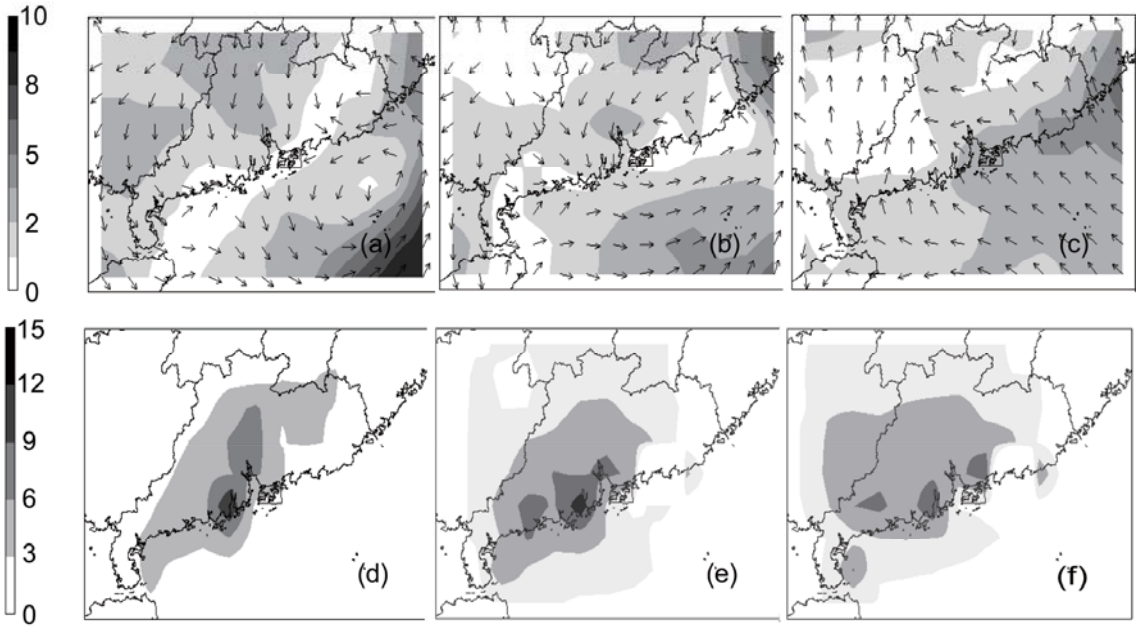

Fig. 3. Modeled wind (vector) and wind speed (shaded, units: m s^{-1}) at 1500 LST for (a) 14 September, (b) 15 September, and (c) 16 September 2004. The increase in surface ozone concentration using adjusted emissions over the estimation of (Street et al., 2003) inventories are shown in (d–f) for the corresponding points of time. (units: ppb)

boundary layer over the PRD region on the first 2 days under the slow northerly wind. Figures 3a–c shows that low wind speed was prevalent in the PRD region and its vicinity during the episode. Light wind and the wind convergence in the PRD region favored the accumulation of precursors and the formation of high O_3 concentration. Most of the O_3 was trapped in the off-coast area over the South China Sea. On the 16 September, the whole PRD region was dominated by a southeasterly wind. Ozone was transported back to the PRD region.

3.2 *Relationship between peak* O_3 *and precursors and impact of temperature increase*

In section 3.1 the base case simulation was reported. The impact of VOC and NO_x emissions are presented in this section. Simulations were repeated 14 times using different VOC or NO_x emissions in each run. The results of the sensitivity tests are listed in Table 1.

3.2.1 *Variation of maximum* O_3 *under different VOC and* NO_x *emission scenarios*

Table 1 shows that when VOC emission were decreased by 90% while NO_x emission was increased to 10 times (case R3), or vice versa (case R4), the O_3 concentration at the ground level was greatly alleviated compared to the base case R7. The daily peak O_3 concentrations at ground level were reduced from 270 ppb to 57 ppb and 67 ppb, respectively, in these runs. That is, surface O_3 was reduced substantially by drastically reducing either VOC or NO_x emissions. When the VOC emissions were constant and that of NO_x was doubled (case R9), the modeled surface ozone concentration peak dramatically increased to 415 ppb. In the extreme case, when VOC and NO_x emissions were increased to 30 and 10 times, respectively, the surface O_3 peak remained at 428 ppb (R13). These results agree well the observed meteorological conditions. When both the surface and air temperatures were enhanced by 10%, peak O_3 concentrations were enhanced in almost all cases (Table 1).

The variations of the O_3 peak with the ratios of FVOC:FNO_x, (FVOC and FNO_x denotes the factors applied to augment or reduce VOC and NO_x emissions for each simulation, respectively), in 15 sensitivity tests under the observed meteorological conditions and the temperature-increase scenario are illustrated in Fig. 4. The hollow markers represent peak O_3 produced under real meterological input; the solid markers represent peak O_3 produced under the temperature-increase scenario. The interesting region in Fig. 4 is where the FVOC:FNO_x ratio is near 0.1. In this region, the temperature-increase scenario increased the daily peak O_3 concentration significantly when the FVOC:FNO_x ratio was between 0.1 and

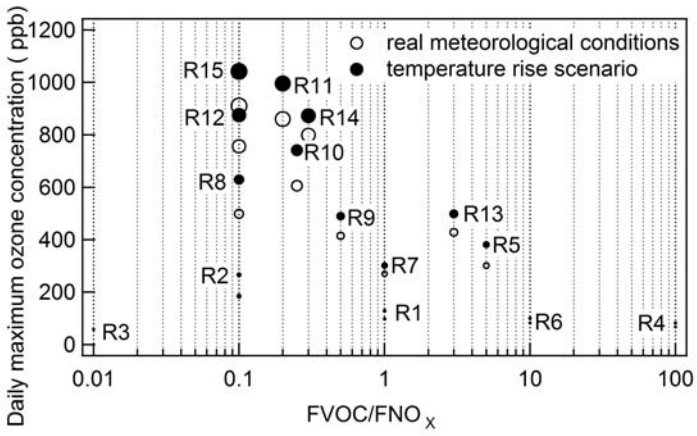

Fig. 4. Variations of modeled daily maximum ozone concentration under real meteorological conditions and temperature-increase scenarios versus FVOC/FNO$_x$ ratio. The marker size is increasingly proportional to the test number from T1 to T15.

0.5. When the ratio was near 0.1, NO$_x$ was abundant during the daytime and O$_3$ was rapidly produced through photolytic reaction with hydroxyl radicals. Altogether, in four cases the FVOC:FNO$_x$ ratio was equal to 0.1: R2, R8, R12, and R15. Only R2 showed a reduction in VOC emissions. The following cases showed substantial increases in NO$_x$ emissions: R8 (an increase to 10 times the base value), R12 (an increase to 20 times), and R15 (an increase to 30 times). The daily maximum O$_3$ concentration increased from 185 ppb (R2) to 270 ppb (R8) to 756 ppb (R12) to 910 ppb (R15). The impact on peak O$_3$ concentration due to temperature increase was smallest when the ratio of FVOC:FNO$_x$ was 0.01 (R3). The daily O$_3$ maximum only changed from 57 ppb to 58 ppb. In case R3, VOC was drastically reduced by 90%, but NO$_x$ drastically increased to 10 times. That is, when FVOC:FNO$_x$ was <0.1, along with the FVOC:FNO$_x$ increased from 0.01 to 0.1, the ozone concentration dramatically increased, which implies that controlling VOCs (decreasing FVOC:FNO$_x$) would reduce ozone concentration. Along with the FVOC:FNO$_x$ range between 0.1 and 10, controlling the NO$_x$ (increasing FVOC:FNO$_x$) would reduce ozone concentration. In conclusion, when the FVOC:FNO$_x$ ratio was <0.1, it was VOC limited, and when the FVOC:FNO$_x$ ratio was between 0.1 and 10, it was NO$_x$ limited. The limiting ratio of FVOC:FNO$_x$ in this study was similar but not the same as that of Toro et al. (2006), which reported a FVOC:FNO$_x$ ratio between 0.5 and 10.

3.2.2 *VOC limited or* NO$_x$ *limited*

Ozone production in photochemical smog processes can be evaluated by plotting the isopleths of maximum O$_3$ concentration. Seinfeld and Pandis (1998) and Palmer et al. (2003) generated O$_3$ isopleths from a number of experiments with photochemical smog chambers. The O$_3$ isopleths allowed the estimation of the sensitivity of the maximum O$_3$ concentrations according to the VOC and NO$_x$ concentrations. Although the pattern of the O$_3$ isopleths was similar in all of the experimental photochemical systems, the shape of the ozone isopleths depends on the specific conditions of radiation, the initial amount of the reactive pollutants, the reaction times, and other variables. To the best of our knowledge, this evaluation has not been applied to the PRD region. Figure 5 displays the peak O$_3$ isopleths as a function of NO$_x$ and VOC emissions at 0600 LST under real meteorological and temperature-increase scenarios.

In the upper-left corner of Fig. 5, the vertical shaving of the O$_3$ isopleths at constant VOC indicates the sensitivity of O$_3$ to VOC emissions. Whereas the horizontal lines on the lower-right corner indicate the corresponding sensitivity to NO$_x$ emissions, when the NO$_x$ emissions were >105.3 kg and the VOC emissions were >106.9 kg, the ozone concentration decreased with VOC increase because of the abundance of VOC. Notably, high O$_3$ concentration (∼800 ppb) occurred when emission of VOC and NO$_x$ were 107.1 kg and 106.2 kg, respectively. Below this ratio, ozone concentration decreased rapidly when NO$_x$ and VOC both decreased.

When the ozone isopleths of the PRD region under real temperature and temperature-increase scenarios were compared (Fig. 5), both scenarios belonged to the NO$_x$-sensitive conditions under current emission levels. If the emissions of VOC and NO$_x$ remain at the current levels, the influence of temperature increase will result in a ∼10% increase in the daily O$_3$

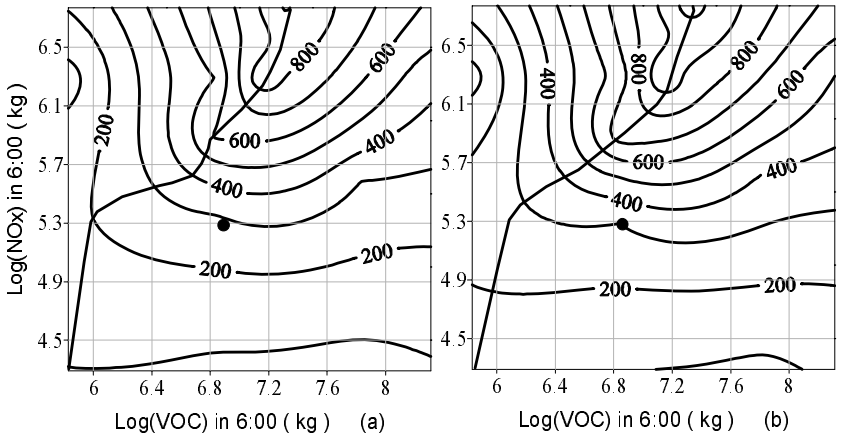

Fig. 5. Maximum ozone concentration isopleths (in ppb) as a function of VOC and NO_x emissions in log space at 0600 LST (in logarithmic scale). The base case is marked with a dot (a) current conditions (b) global warming.

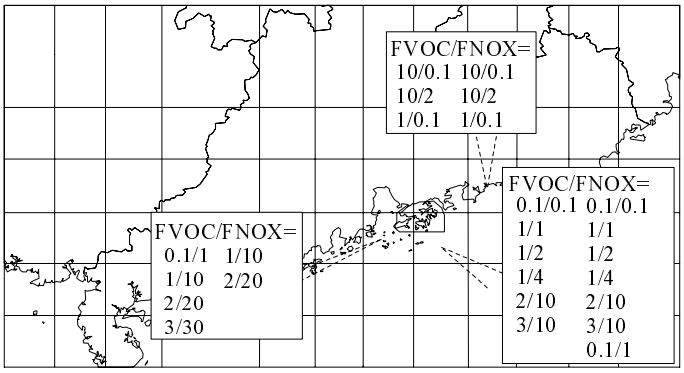

Fig. 6. Locations of the daily maximum surface ozone concentration for different FVOC:FNO_x ratios. Ratios in left and right columns denote observed temperature and temperature-increase scenarios, respectively.

peak concentration. The daily O_3 peak concentration increased under the temperature-increase scenario in all of the simulation runs.

3.2.3 *Effects of temperature rise on locations of maximum* O_3

The locations of daily O_3 peaks in observed temperature and temperature-increase scenarios are shown in Fig. 6. The differences in O_3 peak locations caused by temperature increase were trivial except when FVOC/FNO_x was >1 and at the same time FNO_x was <1. The locations of O_3 peak concentration reside in the PRD region under both scenarios.

3.3 *Estimation of ozone production efficiency and its response to temperature increase*

Ozone production efficiency (OPE) is an important and widely used parameter for evaluating the NO_x emission impact and considering the conditions of O_3 formation. Although many laboratories and modeling studies have reported the basic characteristics of photochemical O_3 formation, a three-dimensional chemical transport model was used to determine how the projected driving forces of emissions and meteorology affect the nonlinear photochemical formation of O_3. In this section, we present the numerical simulation results of ozone production efficiency under observed temperature and temperature-increase scenarios.

OPE can be defined as the number of molecules of oxidants (O_3+NO_2) produced photochemically when a molecule of NO_x (NO+NO_2) is oxidized (Kleinman et al., 2002). The OPE is the number of O_3 molecules produced by oxidation of each NO_x molecule within a parcel of air. Empirically the OPE can be inferred from the regression slope of the observed scatter plot of O_3 concentration versus the concentration of NO_x

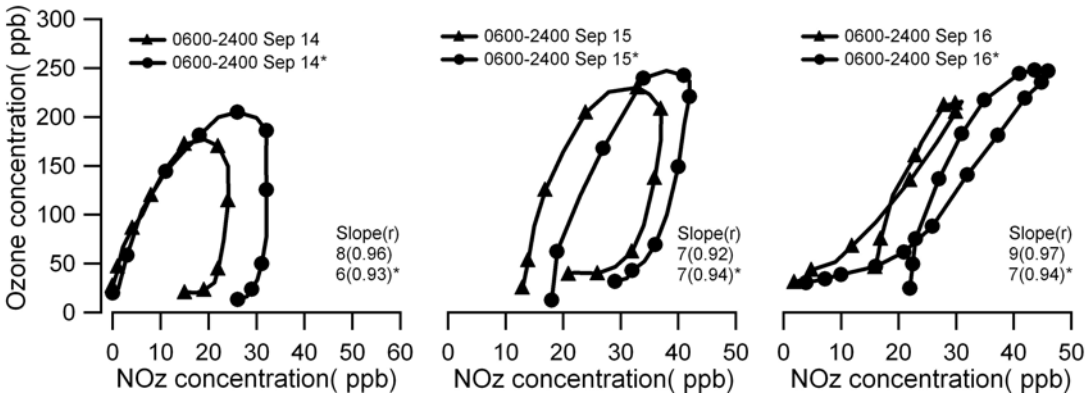

Fig. 7. Scatter plot of modeled O_3 versus NO_z at Tung Chung station (shown in Fig. 1). The line start from grey points at 0600 LST, and the interval between each point is 2 h. Triangle markers denote results using real temperatures and solid circles denote results using the temperature-increase scenario.

oxidation products, that is, NO_z (Trainer et al., 1993). In this study, we used the regression slope of daytime 0700 LST ∼1500 LST) O_3/NO_z as OPE because O_3 tends to be more photochemically active during this period. The NO_z in this study included peroxyacetylnitrate (PAN), nitrous acid (HONO), nitric acid (HNO_3), dinitrogen pentoxide (N_2O_5), and other organic nitrates.

Figure 7 shows the evolution of the relationship between ozone and NO_z on each day, 14, 15, and 16 September 2004 under the observed temperature and the temperature-increase scenario (FVOC:FNO_x ratio). On 14 and 15 September, the O_3 and NO_z were positively correlated in each of these plumes both under observed and warming scenarios before 1500 LST. The regression slopes between 0700 LST and 1500 LST decreased slightly when temperature increase was incorporated. Except for the first few hours on the first day, most of the time during the whole episode, the O_3/NO_z curves under the temperature-increase scenario shifted to the right of the curve associated with the observed temperature scenario (Fig. 7). This result indicates that when temperature increased, higher NO_z concentration was obtained at the same O_3 concentration. Another interesting feature is the positive O_3–NO_z relationship under a temperature-increase scenario that extended to higher NO_z values than were indicated by the observed temperature scenario. This result implies that the crossover point between the NO_x-sensitive conditions and the VOC-sensitive conditions shifted and that the polluted air mass under a warmer environment contained more NO_x before it became an NO_x-sensitive condition.

Using time-dependent Lagrangian modeling, Kleinman et al. (2002) suggested that when a polluted air mass is diluted by background air, OPE increases. This point corroborates the increase of OPE during the episode examined in our study. Furthermore, it has been qualitatively confirmed in several field studies that OPE is inversely dependent on NO_x concentration. Liu et al. (1987) and Lin et al. (1988) were among the first to examine OPE, and they concluded that an NO_x molecule has a higher OPE in clean, remote regions compared with polluted regions. A NO_x molecule could be an order of magnitude more effective in forming O_3 in clean, remote regions (i.e., high OPE) compared with polluted regions (i.e., low OPE). As a matter of fact, NO_x concentrations are relatively low in clean, remote rural areas. At the same time, OPE was found to have a maximum of ∼10 (Trainer et al., 1993; Kleinman et al., 1994; Olszyna et al., 1994). Observations of urban plumes have indicated values of OPE between 3 and 4 in New York City (Kleinman et al., 2000). In the base case of this study, OPE was ∼7–9 under the observed temperature scenario and decreased to ∼6–7 under the temperature-increase

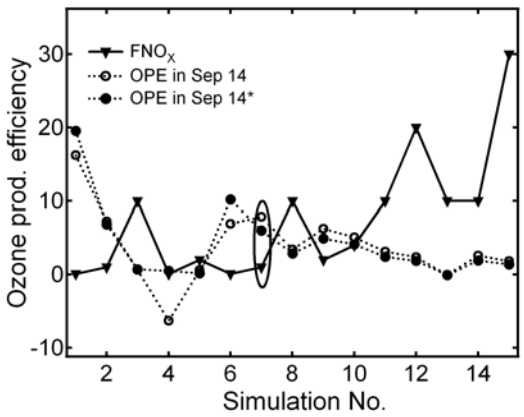

Fig. 8. OPE and FNO_x for each simulation on 14 September. (15 September and 16 September are very similar and therefore were omitted.)

Table 2. OPE calculated at Tung Chung station.

Run no.	OPE			OPE*		
	14 Sep	15 Sep	16 Sep	14 Sep	15 Sep	16 Sep
R1	16	24	20	20	30	23
R2	7	8	10	7	10	10
R3	1	2	1	1	1	1
R4	−6	3	3	1	2	1
R5	1	1	1	0	1	0
R6	7	16	20	10	16	13
R7 (base case)	8	7	9	6	7	7
R8	3	3	3	3	3	3
R9	6	6	7	5	5	6
R10	5	4	6	4	4	5
R11	3	2	3	2	2	3
R12	2	2	2	2	2	2
R13	0	0	0	0	0	0
R14	3	2	3	2	2	2
R15	2	1	1	1	1	1

scenario. This shows a trend of change from NO_x-limited (cleaner, remote air parcel) to VOC-limited conditions (more polluted air parcel). Thus the decrease of OPE under a global warming scenario implies that the extent of pollution in polluted regions has intensified. In case R7 (base case), after 1500 LST on the 16 September, the ozone level decreased quite rapidly; even the NO_z concentration did not change much, and the positive correlation relation between O_3 and NO_z continued even after sunset. To further evaluate this point, OPE was calculated for each day and each simulation run (Table 2). Comparing the results with and without temperature increase, the OPE generally decreased when temperature increased, except for the cases R1 and R2.

Figure 9 shows the OPE distribution (between 0600 LST and 1500 LST) in Guangdong Province during the studied episode. Figures 9a–c displays results under observed temperature scenario, and Figs. 9d–f displays results under a temperature-increase scenario. Low OPE values in the range of 0–5 imply polluted regions, which are marked as light grey. Contours that have negative values of OPE are shown as blank. There are two features in Fig. 9 worth noting. First, the prevailing wind directions were different for the 3 days, namely northerly, southwesterly, and southeasterly winds. Second, the low OPE (polluted region) area was changing during the 3 days. Kleinman et al. (2002) suggested that OPE generally increases with time due to oxidation chemistry and plume dilution. The amount of O_3 produced in a plume depends on the chemical mixing of the plume (abundance of NO_x and VOC and their ratio) as well as the meteorological conditions that affected the dispersion and removal of constituents in the plume. Figure 9 shows that the low OPE area became broader, especially in the PRD region, under the temperature-increase scenario.

4. Conclusions

The sensitivity of O_3 formation was studied using a series of numerical simulations under different NO_x and VOC emission scenarios. Significant reduction in PRD surface O_3 was achieved by drastically reducing either VOC or NO_x by 90%. It appears that abatement in NO_x is more efficient than reduction in VOC, but the results also show that O_3 abatement is not a straightforward issue. The lowest O_3 concentration occurred in case R3, where FVOC was 0.1 and FNO_x was 10. The ozone isopleths of the PRD region showed that they were both NO_x-sensitive with or without temperature increase. When the emission of NO_x was increased ∼4 times ($10^{5.9}/10^{5.3}$), the situation changed to a VOC-limited condition.

When the emission of VOC and NO_x remained unchanged at the current rates, the temperature-increase resulted in an increase of the O_3 peak of 10%. When the emissions of VOC and NO_x were further increased, the daily O_3 peak increased further under the temperature-increase scenario. Thus, in the future, the temperature is expected to increase, and the control policy should account for these changes in meteorology. Our results show that OPE would decrease in the PRD region under the temperature-increase scenario, which implies the presence of more NO_x corresponding to the same ozone levels at higher temperatures. These results also show stronger photochemical production under the warming scenario. However, the locations of daily O_3 peak was not sensitive to the temperature increase; there were only slight differences be-

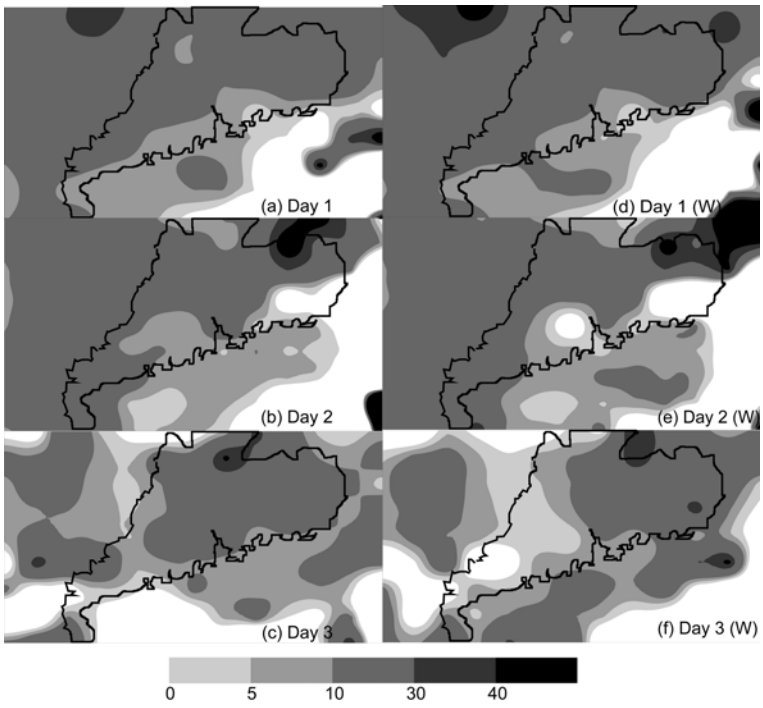

Fig. 9. The spatial distribution of OPE determined as the slope of a regression of modeled Ox and NOz calculated in base case.

tween the two scenarios. Although the spatial patterns were similar, the smog covered a larger area when the temperature increased. In the future, when the temperature increases, more strict control measures are necessary to reduce O_3 concentration.

Acknowledgements. This project was mainly supported by the Hong Kong Research Grants Council (PolyU 5211/09E) and PolyU internal grant (G-U593). This work was partly supported by the National Key Basic Research Development Program of China (Grant Nos. 2010CB428503 and 2011CB403406).

REFERENCES

Byun, D. W., and J. K. S. Ching, 1999: Science algorithms of the EPA Models-3 Community Multiscale Air Quality (CMAQ) modeling system. U. S. Environ. Prot. Agency, Washington, D. C., 727pp.

Carmichael, G. R., and Coauthors0, 2003: Evaluating regional emission estimates using the TRACE-P observations. *J. Geophys. Res.,* **108**, 8810–9926, doi: 10.1029/2002JD003116.

Gery, M. W., G. Z. Whitten, J. P. Killus, and M. C. Dodge, 1989: A photochemical kinetics mechanism for urban and regional scale computer modeling. *J. Geophys. Res.,* **94**, 12925–12956, doi: 10.1029/JD094iD10p12925.

Hogrefe, C., and Coauthors, 2004: Simulating changes in regional air pollution over the eastern United States due to changes in global and regional climate and emissions. *J. Geophys. Res.*, **109**, D22301, doi: 10.1029/2004JD004690.

Houyoux, M. R., J. M. Vukovich, C. J. Coats, N. J. M. Wheeler, and P. S. Kasibhatla, 2000: Emission inventory development and processing for the Seasonal Model for Regional Air Quality (SMRAQ) project. *J. Geophys. Res.*, **105**, 9079–9090, doi: 10.1029/1999JD900975.

IPCC, 2007: *Climate Change 2007—The Physical Science Basis.* Working Group I Contribution to the Fourth Assessment Report of the IPCC Intergovernmental Panel on Climate Change, Cambridge University Press, London, 1056pp.

Jiang, F., T. J. Wang, T. T. Wang, M. Xie, and H. Zhao, 2008: Numerical modeling of a continuous photochemical pollution episode in Hong Kong using WRF-chem. *Atmos. Environ.,* **42**, 8717–8727.

Jiang, F., and Coauthors, 2010: An ozone episode in the Pearl River Delta: Field observation and model simulation. *J. Geophys. Res.,* **115**, D22305, doi: 10.1029/2009JD013583.

Johnson, C. E., W. J. Collins, D. S. Stevenson, and R. G. Derwent, 1999: Relative roles of climate and emissions changes on future tropospheric oxidant concentrations. *J. Geophys. Res.,* **104,** 18631–18645, doi: 10.1029/1999JD900204.

Jacob, D. J., and D. A. Winner, 2009: Effect of climate change on air quality. *Atmos. Environ.,* **43**, 51–63.

Kleinman, L., and Coauthors, 1994: Ozone formation at a rural site in the southeastern United-States. *J. Geo-*

phys. Res., **99**, 3469–3482, doi: 10.1029/93JD02991.

Kleinman, L. I., and Coauthors, 2000: Ozone production in the New York City urban plume. *J. Geophys. Res.,* **105**, 14495–14511, doi: 10.1029/2000JD900011.

Kleinman, L. I., P. H. Daum, Y. N. Lee, L. J. Nunnermacker, S. R. Springston, J. Weinstein-Lloyd, and J. Rudolph, 2002: Ozone production efficiency in an urban area. *J. Geophys. Res.,* **107**, 4733, doi: 10.1029/2002JD002529.

Leung, L. R., and W. I. Gustafson, 2005: Potential regional climate change and implications to US air quality. *Geophys. Res. Lett.,* **32**, L16711, doi: 10.1029/2005GL022911.

Lin, X., M. Trainer, and S. C. Liu, 1988: On the nonlinearity of the tropospheric ozone production. *J. Geophys. Res.,* **93**, 15879–15888, doi: 10.1029/JD093iD12p15879.

Liu, S. C., M. Trainer, F. C. Fehsenfeld, D. D. Parrish, E. J. Williams, D. W. Fahey, G. Hubler, and P. C. Murphy, 1987: Ozone production in the rural troposphere and the implications for regional and global ozone distributions. *J. Geophys. Res.,* **92**, 4191–4207, doi: 10.1029/JD092iD04p04191.

Mickley, L. J., D. J. Jacob, B. D. Field, and D. Rind, 2004: Effects of future climate change on regional air pollution episodes in the United States. *Geophys. Res. Lett.*, **30**, L24103, doi: 10.1029/2004GL021216.

NRC, 1991: Rethinking the ozone problem in urban and regional air pollution. Report of the US National Research Council, Washington, D. C., 524pp.

Olszyna, K. J., E. M. Bailey, R. Simonaitis, and J. F. Meagher, 1994: O_3 and NO_y relationships at a rural site. *J. Geophys. Res.,* **99**, 14557–14563, doi: 10.1029/94JD00739.

Palmer, P. I., D. J. Jacob, D. B. A. Jones, C. L. Heald, R. M. Yantosca, J. A. Logan, G. W. Sachse, and D. G.. Streets, 2003: Inverting for emissions of carbon monoxide from Asia using aircraft observations over the western Pacific. *J. Geophys. Res.,* **108**, 8828, doi: 10.1029/2003JD003397.

Seinfeld, J. H., and S. N. Pandis, 1998: *Atmospheric Chemistry and Physics: From Air Pollution to Climate Change*. 2nd ed., Wiley Publishers, NY, 1326pp.

Steiner, A. L., S. Tonse, R. C. Cohen, A. H. Goldstein, and R. A. Harley, 2006: Influence of future climate and emissions on regional air quality in California. *J. Geophys. Res.,* **111**, D18303, doi: 10.1029/2005JD006935.

Streets, D. G., and Coauthors, 2003: An inventory of gaseous and primary aerosol emissions in Asia in the year 2000. *J. Geophys. Res.,* **108**, 8809, doi: 10.1029/2002JD003093.

Toro, M., V., L. V. Cremades, and J. Calbo, 2006: Relationship between VOC and NO_x emissions and chemical production of tropospheric ozone in the Aburra Valley (Colombia). *Chemosphere,* **65**, 881–888.

Trainer, M., and Coauthors, 1993: Correlation of ozone with NO_y in photochemically aged air. *J. Geophys. Res.,* **98**, 2917–2925, doi: 10.1029/92JD01910.

Wang, T., 2003: Study of visibility reduction and its causes in Hong Kong. Final report to the Environmental Protection Department, Hong Kong Special Administrative Region. [Available at http://www.epd.gov.hk/epd/english/environmentinhk/air/studyrpts/air_studyrpts.html.]

Wang, Y. X., M. B. McElroy, T. Wang, and P. I. Palmer, 2004: Asian emissions of CO and NO_x: Constraints from aircraft and Chinese station data. *J. Geophys. Res.,* **109**, D24304, doi: 10.1029/2004JD005250.

Wang, T. J., K. S. Lam, M. Xie, X. M. Wang, G. Carmichael, and Y. S. Li, 2006: Integrated studies of a photochemical smog episode in Hong Kong and regional transport in the Pearl River Delta of China. *Tellus*, **58B**, 31–40.

Wei, X. L., Y. S. Li, K. S. Lam, A. Y. Wang, and T. J. Wang, 2007: Impact of biogenic VOC emissions on a tropical cyclone related episode in Pearl River Delta Region, China. *Atmos. Environ.,* **41**, 7851–7864.